Manufacturing Rev. **9**, 7 (2022)
© B. Zhou et al., Published by EDP Sciences 2022
https://doi.org/10.1051/mfreview/2022001

Manufacturing Review
Available online at:
https://mfr.edp-open.org

RESEARCH ARTICLE OPEN ACCESS

Fabrication of equiatomic FeCo alloy parts with high magnetic properties by fields activated sintering

Bohao Zhou[1], Yi Yang[1], Yi Qin[2], Gang Yang[1], and Mingxia Wu[1,*]

[1] School of Mechanical Engineering, Sichuan University, Chengdu 610065, P.R. China
[2] Centre for Precision Manufacturing, Dept. of Design, Manufacturing and Engineering Management, The University of Strathclyde, Glasgow G1 1XJ, UK

Received: 2 December 2021 / Accepted: 15 January 2022

Abstract. Electrical field activated sintering technology combined with micro-forming (Micro-FAST), as a new rapid powder sintering/forming method, is used to fabricate FeCo alloy parts. The successfully prepared FeCo parts have a high saturation of 214.11 emu/g and a low coercivity of 16 Oe, and these values are 20% and 10% higher than that of commercially available FeCoV alloy parts on the saturation and coercivity respectively. During the sintering process, the high current application shortened the densification time and enhanced the uniformity of the microstructure significantly. The grain sizes of FeCo alloys were in a range of 5–6 μm, and good isotropy was also shown. The low angle grain boundary (LAGB) accounted for more than 30% and the low angle misorientation accounted for more than 30% of the sample parts. Furthermore, the formation of the nano B2 phase was promoted during the Micro-FAST, and the size of the B2 phase was about 5 nm. The coherent interface between α and B2 was conducive for reducing the coercivity. As a consequence, the outstanding microstructure formed by Micro-FAST makes the FeCo alloys have high saturation and low coercivity.

Keywords: FeCo alloy / electrical field activated sintering / micro-FAST / B2 phase / microstructure

1 Introduction

Iron-cobalt based alloys exhibit excellent magnetic properties such as a high Curie temperature, superior saturation, perfect permeability and low coercivity, which are properties widely desired in high-performance motors, high-density data storage media and micro actuators. The development of FeCo alloys in the past few decades has arisen from the increasing demand for high-performance FeCo alloys for the miniaturization of magnetic parts needed for electromagnetic and information technology [1,2]. However, prohibitively poor ductility and low workability pose challenges to the conventional machining of these materials. Especially for small-size parts where the processing difficulty increases exponentially [3]. Although the ductility can be improved by the addition of vanadium, it will also significantly reduce the permeability and increase the coercivity [4]. With the most suitable addition of vanadium, the magnetic properties of FeCo-2V alloys are still about 10% worse than that of the equiatomic FeCo alloy [5].

Therefore, as a result of previous research [6], near shape processing has become the ideal route for the preparation of micro-size FeCo alloy parts. Silva et al. [7] used powder injection molding (PIM) to eliminate the addition of vanadium and obtained near shape parts with better performance than traditional sintered parts. The saturation of FeCo fabricated by PIM was 2.26T, which was about 10% higher than 1.96T of FeCoV, and permeability was increased from 2677 to 7097 H/m. Albaaji et al. [8] used SPS sintered FeCo with a different sintering temperature to adjust the grain boundary and obtained small grain size parts with measurable magnetic and mechanical properties. The highest saturation of 2.39T was obtained when the grain size was 29.8 μm. Kustas et al. [9] prepared thin-walled FeCo parts with fine grains, uniform structure, and good isotropy through additive manufacturing (Laser Engineered Net Shaping process, open architecture hybrid additive and subtractive manufacturing platform), which achieved an improvement of mechanical properties. The hardness of AM FeCo was more than 150% higher than that of conventionally produced bulk material, and no deterioration of plasticity.

Kustas et al. [9] controlled the distribution of B2 phase by regulating the reaction rate, which can better improve FeCo magnetic performance. Turk et al. [10] enhanced

* e-mail: wumingxia@scu.edu.cn

This is an Open Access article distributed under the terms of the Creative Commons Attribution License (https://creativecommons.org/licenses/by/4.0), which permits unrestricted use, distribution, and reproduction in any medium, provided the original work is properly cited.

mechanical properties (hardness, tensile, and impact toughness were significantly improved) while maintaining the magnetism of FeCo alloy by the introduction of B2 phase. Golchinvafa et al. [11] greatly improved the magnetic properties of FeCo production by the creation of a nano-structured FeCo shell, and obtained the highest saturation of 99 emu/g and lowest coercivity of 450Oe of $CoFe_2O$/FeCo composites powder. Yao et al. [12] introduced in-situ nanoparticles into copper to improve both the physical and mechanical properties of the production. Consequently, the design and introduction of nanostructures are considered to be one of the most useful strategies for the preparation of small-size parts. However, the introduction of B2 phase will result in the deterioration of plasticity [13]. Therefore, it is usually necessary to deform or heat treat the pre-alloyed powder, such as annealing after processing under a disordered bcc state. Kamali et al. [14] treated rolled FeCoV alloys below the transition temperature to eliminate the texture and introduce a small amount of ordered phase. Appropriate heat treatment increased product saturation from 120emu/g to 190emu/g by eliminating processing texture and residue of the high temperature phase. Loureiro et al. [15] annealed FeCo alloy powders at 550°C for 52 hours and ball milled for 150 min, introducing the B2 phase distribution in the sintered product. By studying the phase equilibria in FeCo alloys, Ohnuma et al. [16] predicted that the sufficient formation of B2 phase in bulk samples would require annealing below transition temperature for about 240 h. Sundar and Deevi [13] realized the magnetic enhancement of FeCoV alloys, which were annealed at 600 °C for about 10h by introducing a B2 phase.

The above methods have expanded the industrial application of FeCo alloy, especially the application of field assisted sintering technology such as Spark Plasma Sintering (SPS), which has become a popular method for fabrication of FeCo in industry [17,18]. Except for the Albaaji's work as mentioned above, Yamagishi et al. [19] and Mani et al. [20] also achieved the fabrication of equiatomic FeCo alloy with high saturation (>2.1T) by SPS. The near-shape FeCo parts can be fabricated in about 20 minutes, but they all require post heat treatment to eliminate the negative effect of residual γ phase. The post heat treatment undoubtedly increases time consumption. Therefore, we propose to use Micro-FAST (combining Electrical Field Activated Sintering Technology with Micro-forming) to fabricate high saturation and low coercivity FeCo alloy parts within a much shorter time. Compared with conventional FAST (Field Assisted Sintering Technology), alternating current (ac) is used to generate Joule heat instead of direct current (dc), which is conducive to a uniform distribution of temperature and less time consuming [18–22]. Furthermore, the Micro-FAST process is dedicated to the fabrication of the parts much smaller in sizes than that a conventional sintering method normally dealt with, e.g. the parts with dimensions around 1.0 mm fabricated by Micro-FAST [23]. Wu et al. [24] realized the rapid preparation of TiO_2 by Micro-FAST thus showing that it is a feasible sintering method. Micro-FAST has emerged as a novel process to produce sintered parts via the application of external electrical current and pressure simultaneously in a control manner. The high current application shortens the densification time, thereby making this process a good candidate for sintering FeCo alloys without using additives. However, it is not clear if the microstructural details and properties resulting from a very short, rapid densification are the same in all respects as those resulting from traditional sintering methods.

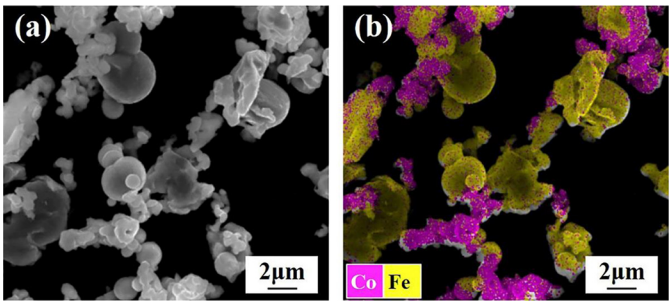

Fig. 1. (a) SEM image of Fe/Co mixed powders. (b) Elements distribution of Fe/Co mixed powders.

In the present work by using the Micro-FAST process we demonstrated a successful fabrication of FeCo micro-components with B2 phase, which have high saturation and low coercivity. By analyzing the phase composition and microstructural characteristics of the FeCo samples, the influence of Micro-FAST on the magnetic properties of the FeCo alloys sintered was studied and the densification mechanism of FeCo alloy parts was examined in detail.

2 Material and methods

Commercial pure Fe powder (99.9% in purity) with an average particle size of 1μm and Co powder (99.99% in purity) with an average particle size of 1μm (Peshing Metal, Jiangsu, China) were selected as the raw materials. A planetary ball mill (QM-QX2, Nanda Instrument, China) was employed to mix the powders. The equiatomic Fe powders and Co powders were mixed by pure ethanol wet milling. 15 mm diameter ZrO_2 balls were used during the wet-milling process, and the weight ratio of ball to powders was 10:1, the jar size was 500ml with a filling ration of 45%. The mixed powders was obtained after running the ball mill at 150 rpm for 6 h. After ball milling, the mixed powders were dried in a drying oven at 97 °C for 1 h. The mixed powders then were preserved by vacuum packaging. A small amount of the mixed powders were placed on a stage with conductive adhesive and excess powders also removed before the scanning electron microscope (SEM) observation. The SEM image of the mixed powder morphology is shown in Figure 1a. It can be seen that the mixed powders have two different morphologies, showing that the Fe powders and Co powders, which are evenly distributed. The size of Fe powders is about 3 μm due to the agglomeration during the mixing. As shown in Figure 1b, the Energy Dispersive Spectrometer (EDS) result indicates that the mixed powders consist of

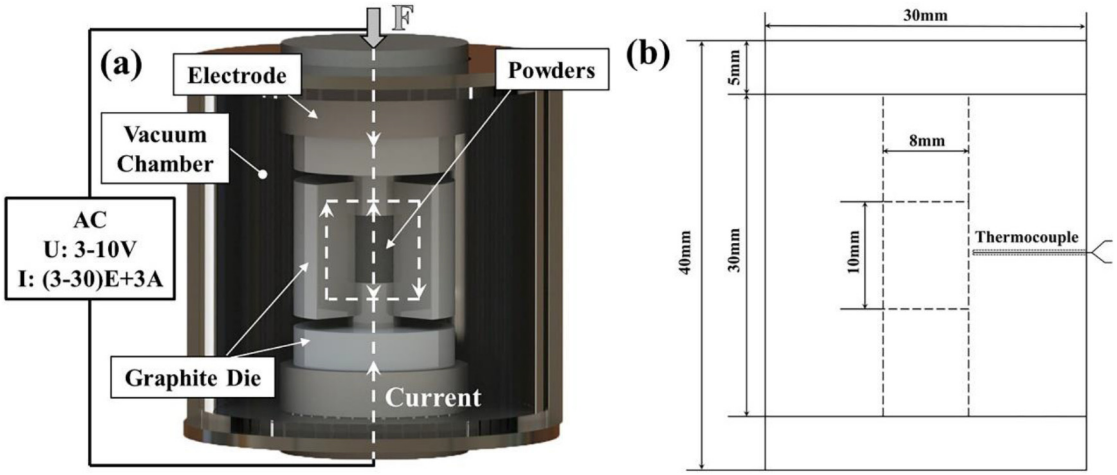

Fig. 2. (a) Schematic diagram of the FeCo fabrication by the Micro-FAST process. (b) Size of Micro-FAST dies.

pure Fe and Co powders, and no mechanical alloying and oxidation happened during preparation of the mixed Fe/Co powders.

The schematic diagram of the FeCo fabrication by the Miro-FAST process is shown in Figure 2a. Without any special pretreatment, the mixed powders are directly placed into the graphite die cavity with a diameter of 8 mm and height of 10 mm. The size of the die is shown in Figure 2b. The sintering process is carried out in a Gleeble-1500 D thermal simulation instrument. The powder system is settled uniaxially under a force of 50 MPa, the vacuum level in the chamber reached 10^{-3} Pa, and the alternating current (AC) is applied from the electrode at both ends of the graphite die. The current intensity is about (3–30)E+3A, the voltage intensity is about 3–10 V. The thermocouple device is attached in a drilled hole in the die wall as shown in Figure 2b. The depth of the hole is about 8 mm and the thermocouple is used to measure and adjust the sintering temperature. With a heating rate of 5 °C /s, the system was heated to 900 °C and 1100 °C, and maintained for 3 min. The temperature ramp rate is determined from a previous study of Micro-FAST. In this work, the heating process is relatively steady which makes the powders heat uniformly. Based on pre-experiments of fabrication of FeCo by using Micro-FAST, we set 900 °C as the sintering temperature. Usually, the hold temperature of SPS is 1100 °C, we also use this sintering temperature to study the effect of lower energy input and shorter processing time. Finally, the applied current was reduced and the pressure was released simultaneously, and the sample was cooled down to room temperature. Figure 3 shows the plots of the thermal profile as a function of time.

For reliability of experimental results, we show two samples obtained at the same sintering temperature in some characterizations. X-Ray diffraction (XRD, Co $K_{\alpha 1}$ radiation with a wavelength of $\lambda = 0.178896$ nm, step size was 0.02°) was carried out to collect XRD patterns from the samples to examine their phase composition. The hysteresis loops of the samples were obtained by Physical Property Measurement System (PPMS, Quantum Design) with the applied field of 25000Oe. Two samples sintered with the same parameters were tested in different directions – one parallel

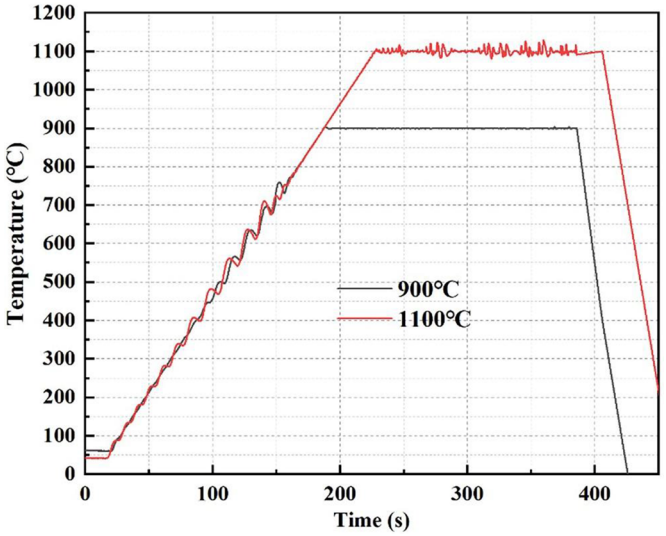

Fig. 3. Thermal profile as time with different sintering temperature.

to the axis and one vertical to the axis, to avoid the potential effect of anisotropy. The Archimedes method was used to investigate the density of samples. The microstructure of the FeCo was characterized by the scanning electron microscope (SEM, 20kV) equipped with Energy Dispersive Spectroscopy (EDS, JSM-IT300). Microstructural characterization of the samples was conducted using Transmission Electron Microscope (TEM, FEI F20) with EDS detector and Electron-backscatter diffraction (EBSD, HKL symmetry, step size was 0.1 μm). The EBSD data points with a confidence index below 0.2 were removed, which was about 2% EBSD data points.

3 Results and discussion

3.1 Magnetic properties

The hysteresis loops of FeCo fabricated by the Micro-FAST are shown in Figure 4. All samples exhibit high saturation (Ms) and low coercivity (Hc), which are typical

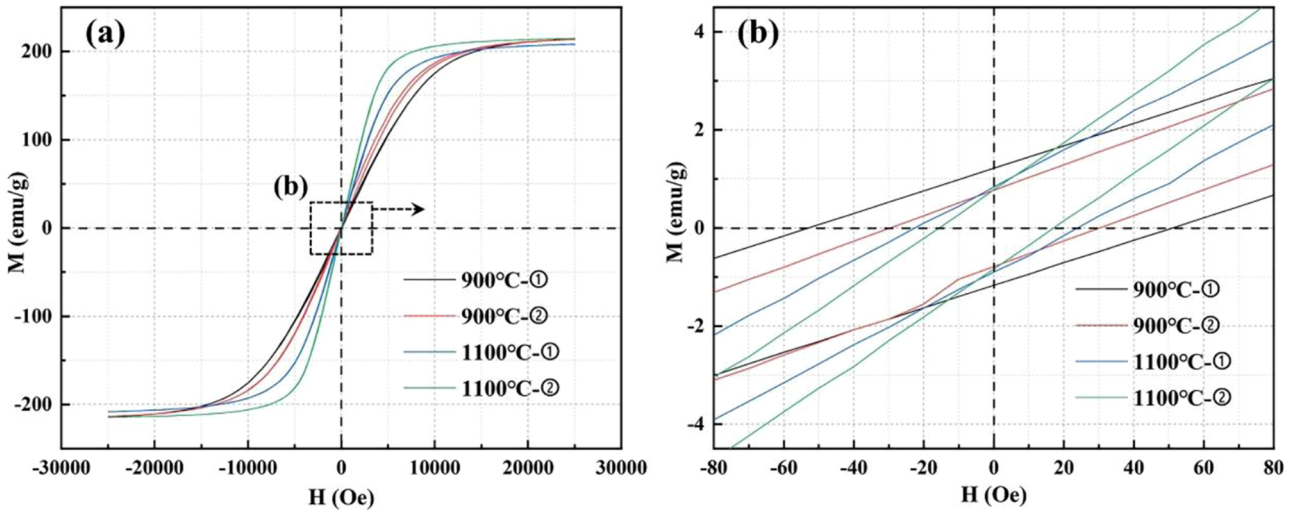

Fig. 4. (a) Hysteresis loop of FeCo fabricated by the Micro-FAST and (b) Enlargement of the area near the origin.

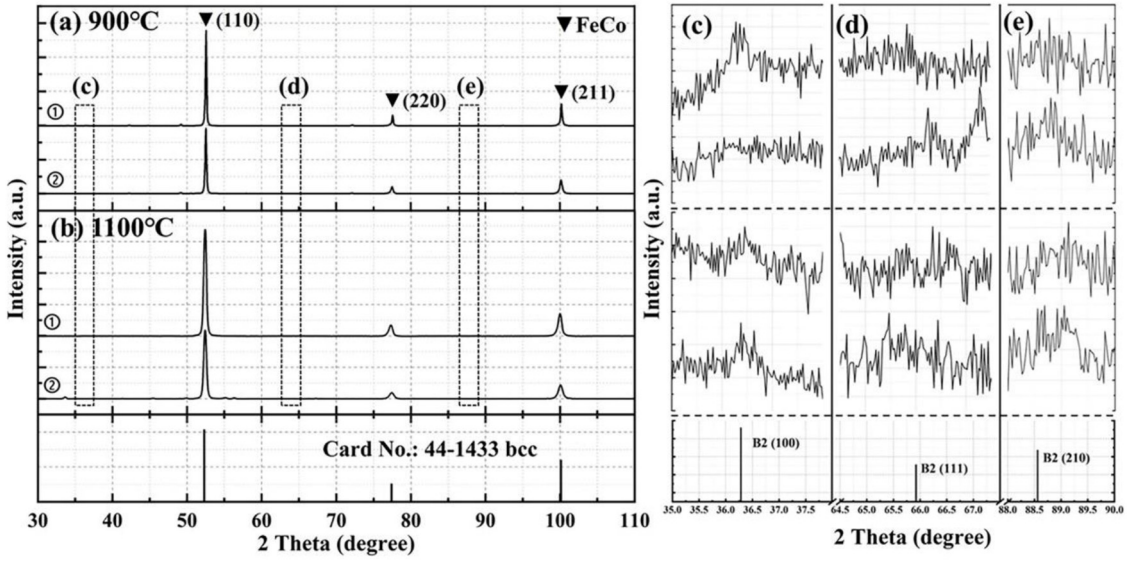

Fig. 5. X-Ray diffraction patterns of the FeCo samples sintered at (a) 900 °C and (b) 1100 °C, (c)-(e) the enlarged view in the degree range of appearance of B2 reflections.

magnetic characteristic of FeCo alloys. The hysteresis loops are so narrow that the coercivity cannot be clearly identified, therefore an expansion of the region near the origin is given in Figure 4b. The Ms of the two samples sintered at 900 °C are 213.42 emu/g and 214.11 emu/g, and Hc are 53 Oe and 30 Oe, respectively. For samples sintered at 1100 °C, the Ms are 208.19 emu/g and 214.66 emu/g, and Hc are 23 Oe and 16 Oe respectively. With the increase of the sintering temperature, the Ms of all samples is similar, but the Hc decreases significantly. The largest decrease of Hc reaches 69.8%, which is a favorable performance for FeCo alloy to reduce the energy loss in industrial application. This criterion refers to the Liang's research [25] on the reliability for the criteria for the glass-forming ability and corresponding magnetic properties, because the microstructure of FeCo alloy fabricated by Micro-FAST in the presented study is similar to that for the FeCo alloys reported from the Liang's research.

3.2 Phase and microstructure

Figure 5 shows the XRD patterns of the FeCo samples fabricated by the Micro-FAST process. The XRD patterns show that the FeCo alloy with a typical BCC structure was fabricated at both 900 °C and 1100 °C, and the FeCo samples are fully dense with a relative density higher than 99%. Apparently, the patterns consist only of the fundamental lines for a BCC lattice, but B2 lattice reflections are evidenced when zooming on the two theta ranges (Fig. 5c,d,e), where they are expected to appear.

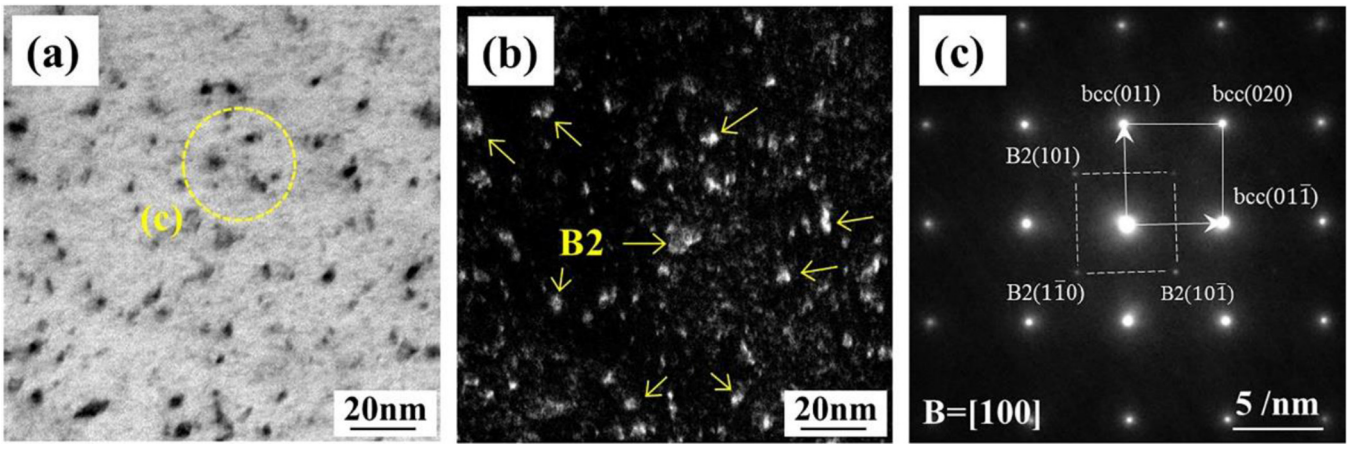

Fig. 6. TEM of FeCo sample sintered at 900 °C, (a) bright-field image of microstructural morphology. (b) dark-field image of microstructural morphology. (c) SAED obtained from white area in (a).

The identification of B2 lattice refers to Ohnuma et al. [16] research on equilibrium phases of a FeCo binary system. According to Ohnuma's work on equilibrium phases of the FeCo binary system, the intensity characteristic peaks (111) and (210) of B2 are much lower than the peak (100). From Figure 5c, the intensity of B2(110) shows a similar intensity degree as the previous study. Although the B2 lattice cannot be strongly displayed on the patterns due to its low content, small size, and small detected area, it provides a basis for further microscopic characterization.

To further confirm the existence of a B2 phase, Transmission electron microscope (TEM) characterization is carried out to study the microstructure of the samples. Figure 6 shows the TEM images of the FeCo sample sintered at 900 °C. It can be seen that the dark nanophases with a size of 10nm or less are distributed in the matrix. The SAED pattern in Figure 6c reveals an obvious diffraction spot of B2 lattice and BCC FeCo matrix. And the dark field image is obtained from the B2(011) diffraction spot. According to the dark-field image in Figure 6b, we can determine the distribution and size of the B2 phase in matrix, as indicated by the yellow arrow. With a size of 5nm, the B2 phase uniformly distributes in the FeCo matrix. Han et al. [26] controlled the anisotropy in single grain of bulk FeCo to introduce nanoinclusions of 3–5 nm to obtain higher saturation. MacLaren et al. [27] used the layer Korringa-Kohn-Rostoker method to study the electronic-structure of B2 and matrix from first-principles, and confirmed that the existence of the B2 phase is beneficial to the reduction of coercivity. Hence, the existence of the nano-B2 phase is beneficial for increasing the saturation and reducing the coercivity. Micro-FAST can introduce a nano-B2 phase during the process without any special treatment.

Figure 7 is the High-Resolution transmission electron microscopy (HRTEM) images of FeCo sample sintered at 1100 °C. Figure 7a is the detected area. The FFT image of this area is shown in Figure 7e, and the diffraction spots of the B2 lattice can be clearly distinguished. Figure 7c is obtained by inverse FFT from the B2 diffraction spots

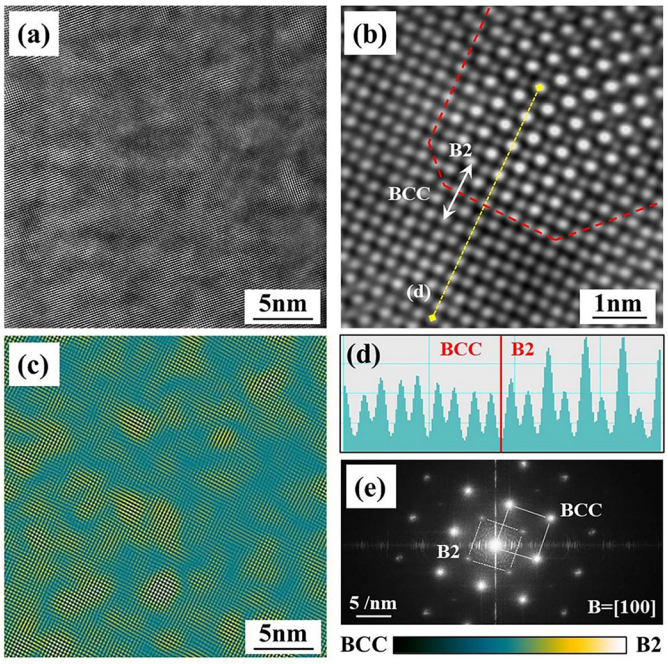

Fig. 7. (a) HRTEM of FeCo sample sintered at 1100 °C along the [100], (b) interface between α and B2, (c) Inverse FFT image of detected area, (d) line intensity profiles of the atomic columns measured along <001> direction, (e) FFT image of detected area.

mask. The IFFT image indicates that the B2 phase distributes more uniformly in the sample sintered at 1100 °C. Figure 7b is a higher magnification of a B2 ordered region adjacent to a disordered α region. The corresponding atomic column intensity profile, across the disordered α/ordered B2 interface, is shown in Figure 7d. The alternating column intensities in the B2 region establish the ordered nature of this region, while all atomic column intensities are nominally equal in the disordered α region. Figure 7b shows a neat coherent interface between α and B2, which is beneficial to reduce coercivity. Tôkei et al [28].

According to the interface between B2 and the matrix, it can be known that the coherent interface is more conducive to the reduction of coercivity.

To further indicate the microstructure characteristics, SEM and TEM observations were performed. As shown in Figure 8a, there are many dispersed cubic pores in the sample. Based on the geometry of these pores, we believe that this is caused by the shedding of cubic FeCo nanoparticles during the preparation of the test sample. Kazakova et al. [29] showed that $Fe_{2(66)}Co_{(33)}$ had a tendency to form lath complexes. Mohapatra et al. [30] expressed the tendency of FeCo shells to form specific geometric shapes on the nanoscale by preparing self-assembled FeCo shell particles. From the TEM image in Figure 8b, BCC structure FeCo nanoparticles with a size of 100~200 nm are found. The chemical composition of these nanoparticles is about Fe55:Co45 from the EDS result, also, the chemical composition of the edge of corrosion pores in Figure 8a is Fe45:Co55, which is consistent with the previous studies. Arief and Mukhopadhyay [31] prepared $Fe_{55}Co_{45}$ nanoparticles with extremely good cubic shape by controlling the element ratio during the chemical synthesis. In addition, the fact that Garnero et al. [32] prepared FeCo nanoparticles with a B2 ordered lattice by co-decomposing two metal-amide precursors under mild conditions also indicates the similar formation process of both cubic particles and nano B2 phase under certain conditions. During the Micro-FAST process the current flows uniformly through the powder system. However, at the initial stage of sintering the local high temperature caused by electrothermal focusing at the particle contact area will promote more nucleation cores during crystallization. Meanwhile the pressure during the Micro-FAST process also promotes the breaking of big agglomerations of mixed powders, especially irregularly shaped Co powders, into small particles and compressing them which increases the contact area between powders. This larger contact interface promotes a more uniform current flow through the powders and the diffusion of Fe and Co elements.

Figure 9 shows the EBSD results of FeCo samples sintered at 900 °C and 1100 °C. From the IPF on X0 plane as shown in Figure 9a,b, it can be seen that FeCo samples sintered at 900 °C and 1100 °C are composed of uniform fine grains. The grain size of the latter is 6.07 μm, which is larger than the 5.26 μm of the former. The increase of grain size is mainly due to the grain growth caused by higher sintering temperature. The fine grain of the FeCo sample fabricated by the Micro-FAST process is an essential factor for the high Ms and low Hc. Liu et al. [33] investigated FeCo alloys microstructure evolution and corresponding magnetic properties under different undercooling degrees. This revealed that the grain refinement was shown to be conducive to improved magnetic properties of FeCo alloys. As shown in Figure 9c,d, the samples are mainly composed of FeCo alloy with BCC structure. Although B2 phase also has the BCC structure, and the size of the B2 phase is less than 10 nm, which is much smaller than the step size of 100 nm, it is difficult to catch the appearance of B2 phase.

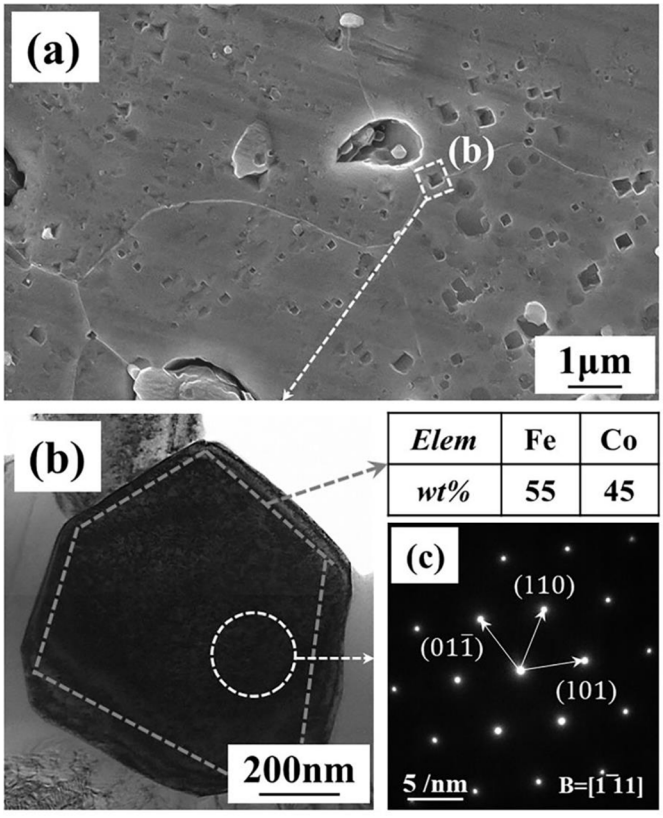

Fig. 8. (a) SEM image of FeCo sample sintered by Micro-FAST, (b) TEM image of FeCo nanoparticles, (c) SAED obtained from the FeCo nanoparticle.

From the pole diagram of the FeCo samples, it can be seen that the samples do not have an obvious preferred orientation and show good anisotropy. On the one hand, it is ensured that the samples exhibit close Ms in each test direction. On the other hand, the test results of the sample shown in Figure 5 can represent the performance in all directions. The grain boundary and the uniformity are important factors affecting the Hc [34], ahigh angle grain boundary (HAGB) will lead to an increase of Hc. Li et al. [35] eliminated the HAGB by annealing to reduce the coercivity of the samples. Yu et al. [36] studied the pinning effect of the grain boundary on the magnetic domain wall movement, and proved that the HAGB will more strongly restrict the movement of the magnetic domain wall. As shown in Figure 9g, the grain boundaries of the 900 °C and 1100 °C sintered samples are mostly low angle grain boundaries (LAGB). With the sintering temperature increases, the proportion of LAGB is further increased. Meanwhile, the local misorientation distribution is used to represent the micro-uniformity in the grain interior. It can be seen from Figure 9h, the samples show a concentration on a low misorientation angle. With the increase of sintering temperature, the misorientation distribution is concentrated at a lower angle which is considered to be an improvement of micro-uniformity. The enhancement of the

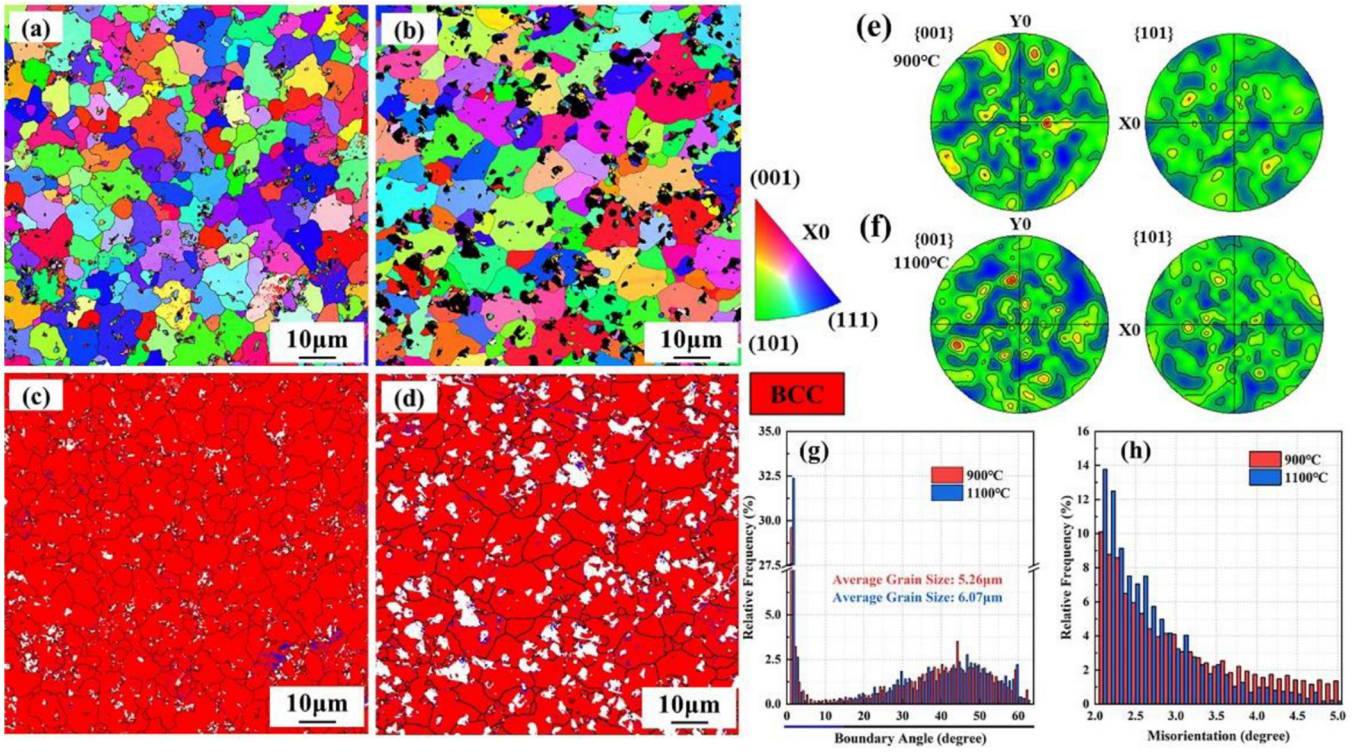

Fig. 9. IPF images of FeCo sintered at (a) 900 °C and (b) 1100 °C, (c), (d) phase composition and grain boundary (LAGB is shown in blue line) of FeCo samples, (e), (f) pole Fig. of FeCo samples. (g) grain boundary angle distribution of FeCo samples, (h) local misorientation distribution of FeCo samples.

micro-uniformity also has a positive effect on the decrease of coercivity. Hasani et al. [37] and Kustas et al. [9] studied the properties of rolled and extruded FeCo alloys, they found that a certain texture will improve the saturation of FeCo products in a specific direction, but it also significantly increase the coercivity.

3.3 Sintering mechanism

During the Micro-FAST sintering process, the current uniformly passes through the powder system. Wu et al. [38] studied the different stages of Micro-FAST densification through detailed TEM, showing that the electric current and pressure distribution are two unique characteristics of Micro-FAST. The uniform temperature distribution makes each particle show a similar trend of growth during the densification. As a result, the fabricated bulk FeCo has uniform grain size distribution and good anisotropy. With the sintering temperature increased from 900 °C to 1100 °C, the heating and cooling stages are prolonged by about 1 minute, providing more time for grain growth. Meanwhile, the LAGB, with higher energy storage, is promoted by higher energy input. The activity and time of atomic diffusion are improved by the higher temperature which is also conducive to micro-uniformity. Fine grain, good anisotropy, LAGB and better micro-uniformity assist in reducing the energy loss of the FeCo alloy during the magnetic induction.

Based on the results of microstructural characterizations, we proposed a densification mechanism of FeCo alloy fabricated by Micro-FAST. Figure 10 is the schematic diagram of the sintering process of Micro-FAST and the state of grain boundaries and grain interior. During the sintering process, the alternating current continuously passes through the powder system. Except for the heat transferred from the heated mold to the powders, the current directly passing through the mixed powders will

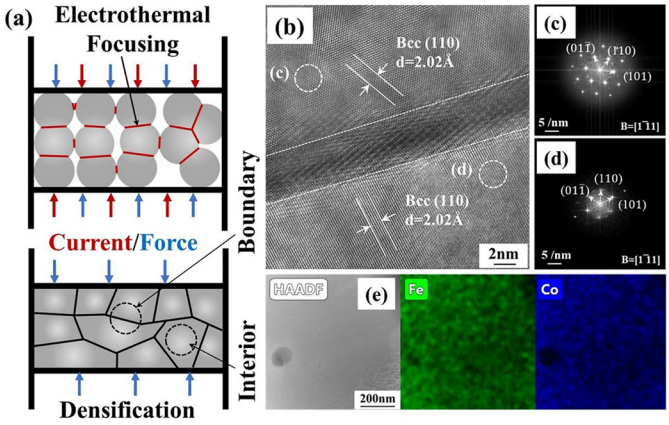

Fig. 10. (a) Schematic diagram of densification process of the Micro-FAST. (b) HRTEM of FeCo grain boundary, *d* indicates lattice spacing. (c) and (d) FFT image of grains from grain boundary. (e) HAADF and surface chemical composition of grain interior.

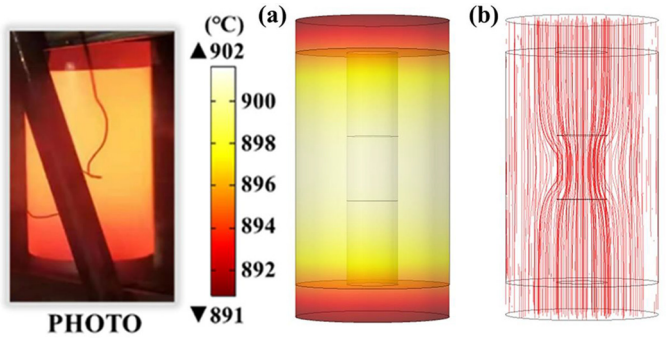

Fig. 11. Photo and simulation of (a) temperature distribution, and (b) simulation of current distribution during Micro-FAST.

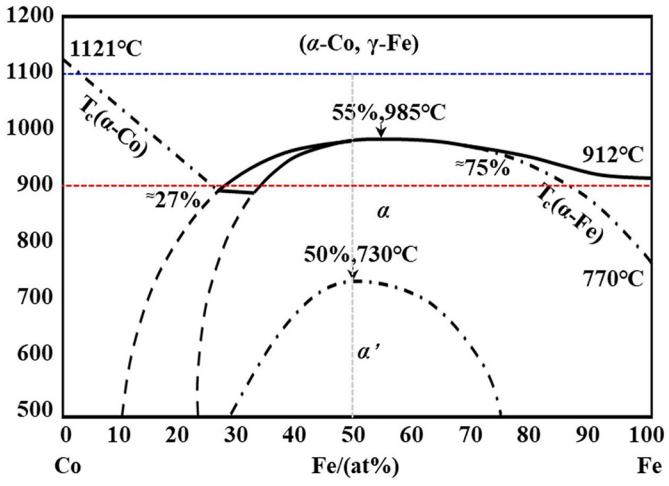

Fig. 12. Co-Fe phase diagram, red and blue lines are the sintering temperature in the presented study, 900 °C and 1100 °C respectively.

also generate a large amount of Joule heat and raise the temperature. Importantly, the mixed powders is not completely dense before sintering, the current path is the contact surfaces between the particles. The small contact area between the particles with higher resistance will become a location for thermal accumulation during the sintering, this is called electrothermal focusing [24,38,39]. The contact part of the particles will be heated to a high temperature which may exceed the melting point. Under the loading force, the densification process of the powders is accelerated. Figure 10b is the HRTEM of the FeCo fabricated by Micro-FAST, the boundary is dense and neat. The FFT obtained from side of the boundary is shown in Figure 10c,d. The FFT indicates the formation of BCC FeCo alloy. As shown in Figure 10e, the HHADF of the grain interior shows uniform contrast, and Fe, Co elements distributed uniformly, indicating the good uniformity of the grain interior.

To analyze the heat effect of fabrication of FeCo by Micro-FAST a simulation was carried out to examine temperature and current distribution, this is shown in Figure 11. The temperature distribution is not uniform in powders and die because of different current resistance. There is a stronger current through powders because of its higher conductivity. The simulation is consistent with Garay et al. work on FAST/SPS. [40,41] Although we can't detect the temperature of powders directly, we can estimate it by simulation because the surface temperature distribution of the die is consistent with simulation as shown in the photo in Figure 11. The simulation indicates that temperature distribution is relatively uniform in the powder itself. Therefore, the drilling hole to attach the thermocouple is as deep as possible so that the thermocouple can reflect the powder's temperature as accurately as possible. The uniform temperature distribution is conducive to uniform densification and diffusion of the mixed powders.

According to the phase diagram as shown in Figure 12, which refers to the work from Okamoto and Massalski [42], it can be determined that during the Micro-FAST process, the densification of FeCo alloy from pure Fe and Co mainly relied on the atom diffusion. In the presented work, the hold sintering temperature is set at 900 °C and 1100 °C, which is much lower than molten temperature of Fe and Co. Even if the electrothermal focusing can induce the high temperature to form a local liquid phase area, the high temperature region is small and the hold time is too short to cause every particle to be melted, so atom diffusion still plays a major role in alloying. As shown in the Nitta et al. [33] work on diffusion of Fe and Co, the diffusion at such a sintering temperature is high enough to achieve full alloying in such a short time. Considering powders size, the contact area between powders is very large and this is conducive to interatomic diffusion during the Micro-FAST process. The XRD and TEM results show that the equiatomic FeCo alloy fabricated by Micro-FAST is a typical BCC (α) structure, and there is no residual pure Fe or Co, indicating that the interatomic diffusion during the process is enough to homogenize the FeCo alloy.

As for the formation of B2, two characteristics of Micro-FAST promote the formation of B2 in equiatomic FeCo alloy. On the one hand, the loading force on the powder system not only compacts the mixed powders at the initial stage of sintering but also causes the deformation of the particles. In the contact area of the particles, the area where atom diffusion occurs first, is also the area where deformation is strongest. As thermodynamics is considered, B2 is particularly stable at lower temperature. However, as Jeffery stated [43], when the applied force and powders size are concerned, B2 can be formed at a higher temperature than its transition temperature. Also, if the alloying of FeCo is achieved by diffusion at the nano scale, the FeCo alloy will strongly preferentially stack in the (001) direction under the influence of surface energy. Under a slow temperature ramp rate the ordering kinetics are accelerated by the surface-diffusion-driven coarsening in the nonporous surface [44]. The kinetic paths of ordering B2 phase are independent of temperature with a nano-size grain. This provides short-circuited diffusion paths for atom movements to form the nano B2 phase [45,46]. So,

these areas provide favorable conditions for the formation of nano B2 phase during the Micro-FAST process. On the other hand, during the sintering, the temperature of the powder system is uniformly increased by the continuing current, but the overall low sintering temperature makes about 50∼60% of the entire fabrication time in the annealing range. Also, the low temperature change rate further promotes the formation of the nano B2 phase in equiatomic FeCo alloy fabricated by the Micro-FAST.

4 Conclusions

Through the research reported in this paper, FeCo alloys with excellent magnetic performance were fabricated successfully with a Micro-FAST process at lower sintering temperatures. The main conclusions can be drawn from this research:

- Micro-FAST would enable densification of FeCo alloys rapidly. During the process, the local high temperature caused by the electrothermal focus promotes the formation of a dense grain boundary from the particle interface and also promotes the diffusion between different atoms to form good micro-uniformity.
- The FeCo alloys fabricated by the Micro-FAST have fine grain sizes of 5–6 μm. These show good isotropy. The low angle grain boundary accounts for more than 30% of the sample parts and the low angle misorientation accounts for more than 30%. These microstructural characterizations cause the samples to have both high Ms and low Hc.
- Nano B2 phase is distributed in the FeCo fabricated by the Micro-FAST without any treatment, and the size of the B2 phase is about 5nm. The coherent interface between BCC and B2 is conducive to the reduction of the coercivity.

The results presented in this paper demonstrate Micro-FAST to be an advanced powder metallurgy method able to efficiently fabricate uniform microstructures and dispersed B2 nano phases, especially for the fabrication of small-sized bulk FeCo components. However, how to control the size and distribution of these phases is still of great challenges, especially considering applications of the technology in a production environment.

Declarations of competing interests

On behalf of all authors, the corresponding author states that there is no conflict of interest.

Funding Information

The research reported in this paper has been supported by National Natural Science Foundation of China (Grant No. 51675357).

References

1. T. Sourmail, Near equiatomic FeCo alloys: Constitution, mechanical and magnetic properties, Prog. Mater. Sci. **50** (2005) 816–880
2. J.E. May, M.F. de Oliveira, S.E. Kuri, New highly magnetic and oxidation-resistant FeCo-based alloys, Mater. Sci. Eng. A **361** (2003) 179–184
3. J.M. Silveyra, E. Ferrara, D.L. Huber, T.C. Monson, Soft magnetic materials for a sustainable and electrified world, Science **362** (2018)
4. K. Kawahara, Effect of additive elements on cold workability in FeCo alloys, J. Mater. Sci. **18** (1983) 1709–1718
5. B. Nabi et al., Effect of recrystallization and degree of order on the magnetic and mechanical properties of soft magnetic FeCo-2V alloy, Mater. Sci. Eng. A **578** (2013) 215–221
6. Y. Sakka, T. Uchikoshi, E.J. Ozawa, Sintering characteristics of Fe and FeCo alloy ultrafine powders, Mater. Sci. **28** (1993) 203–217
7. A. Silva, J.A. Lozano, R. Machado, J.A. Escobar, P.A.P. Wendhausen, Study of soft magnetic iron cobalt based alloys processed by powder injection molding, J. Magn. Magn. Mater. **320** (2008)
8. A.J. Albaaji, E.G. Castle, M.J. Reece, J.P. Hall, S.L. Evans, Synthesis and properties of graphene and graphene/carbon nanotube-reinforced soft magnetic FeCo alloy composites by spark plasma sintering, J. Mater. Sci. **51** (2016) 7624–7635
9. A.B. Kustas et al., Controlling the extent of atomic ordering in intermetallic alloys through additive manufacturing, Addit. Manuf. **28** (2019) 772–780
10. C. Turk et al., Impact of the B2 ordering behavior on the mechanical properties of a FeCoMo alloy,Mater. Sci. Eng. A **662** (2016) 511–518
11. S. Golchinvafa, S.M. Masoudpanah, M. Jazirehpour. Magnetic and microwave absorption properties of FeCo/$CoFe_2O_4$ composite powders, J. Alloys Compd. **809** (2019) 151746
12. G. Yao, S. Pan, J. Yuan, Z. Guan, X. Li, A novel process for manufacturing copper with size-controlled in-situ tungsten nanoparticles by casting, J. Mater. Process. Tech. **296** (2021) 117187
13. R.S. Sundar, S.C. Deevi, Effect of heat-treatment on the room temperature ductility of an ordered intermetallic Fe-Co-V alloy, Mater. Sci. Eng. A **369** (2004) 164–169
14. M.R. Kamali et al., Influence of microstructure and texture evolution on magnetic properties attained by annealing of a cold-rolled Fe-Co-10V semi-hard magnetic alloy, Mater. Charact. **169** (2020) 110591
15. J.M. Loureiro, A.C. Batista, V.A. Khomchenko, B.F.O. Costa, G. Le Caër, Order-disorder phenomena from X-ray diffraction in FeCo alloys annealed and ground at high energy, Powder Diffr. **26** (2011) 267–272
16. I. Ohnuma et al., Phase equilibria in the Fe-Co binary system, Acta Mater. **50** (2002) 379–393
17. V. Mamedov, Spark plasma sintering as advanced PM sintering method, Powder Metall. **45** (2002) 322–328
18. Z.Y. Hu et al., A review of multi-physical fields induced phenomena and effects in spark plasma sintering: Fundamentals and applications, Mater. Des. **191** (2020) 108662
19. W. Yamagishi, K. Hashimoto, T. Sato, S. Ogawa, Z. Henmi, Magnetic properties of Fe-Co alloys produced by powder metallurgy, IEEE Trans. Magn. **22** (1986) 641–643
20. M.K. Mani, G. Viola, M.J. Reece, J.P. Hall, S.L. Evans, Mechanical and magnetic characterisation of SiC whisker reinforced Fe-Co alloy composites, Mater. Sci. Eng. A **592** (2014) 19–27

21. M. Ze'ev Becker, N. Shomrat, Y. Tsur, Recent Advances in Mechanism Research and Methods for Electric-Field-Assisted Sintering of Ceramics, Adv. Mater. **30** (2018) 1–8
22. N.S. Weston, B. Thomas, M. Jackson, Processing metal powders via field assisted sintering technology (FAST): a critical review, Mater. Sci. Technol. (United Kingdom) **35** (2019) 1306–1328
23. A. Du, Y. Yang, Y. Qin, G. Yang. Effects of Heating Rate and Sintering Temperature on 316L Stainless Steel Powders Sintered under Multiphysical Field Coupling, Mater Manuf Process, **28** (2013) 66–71
24. M. Wu, Y. Yang, G. Yang, D. Yin, Fabrication of TiO2 components by Fields Activated Sintering Technology (FAST), Ceram. Int. **43** (2017) 8075–8080
25. X. Liang, T. Erenc-Sedziak, M. Kowalczyk, T. Kulik, B. Xu, Evaluation on the reliability of criterions for glass-forming ability of Fe(Co)-based bulk metallic glasses, J. Mater. Process. Technol. **204** (2008) 465–468
26. Z. Han et al., P-tridoped bamboo-like carbon nanotubes decorated with ultrafine Co_2P/FeCo nanoparticles as bifunctional oxygen electrocatalyst for long-term rechargeable Zn-air battery, J. Colloid Interface Sci. **590** (2021) 330–340
27. J.M. MacLaren, T.C. Schulthess, W.H. Butler, R. Sutton, M. McHenry, Electronic structure, exchange interactions, and Curie temperature of FeCo, J. Appl. Phys. **85** (1999) 4833–4835
28. Z. Tôkei, J. Bernardini, D.L. Beke, Grain-boundary diffusion in B2 intermetallic compounds: Effect of ordering on diffusion in the Fe_3Al and FeCo compounds, Acta Mater. **47** (1999) 1371–1378
29. M.A. Kazakova et al, Structural and electromagnetic properties of Fe2Co-multi-walled carbon nanotubes-polystyrene based composite, J. Alloys Compd. **844** (2020) 156107
30. J. Mohapatra, M. Xing, J. Elkins, J.P. Liu, Hard and semi-hard magnetic materials based on cobalt and cobalt alloys, J. Alloys Compd. **824** (2020) 153874
31. I. Arief, P.K. Mukhopadhyay, Preparation of spherical and cubic $Fe_{55}Co_{45}$ microstructures for studying the role of particle morphology in magnetorheological suspensions, J. Magn. Magn. Mater. **360** (2014) 104–108
32. C. Garnero et al., Chemical Ordering in Bimetallic FeCo Nanoparticles: From a Direct Chemical Synthesis to Application As Efficient High-Frequency Magnetic Material, Nano Lett. (2019) doi:10.1021/acs.nanolett.8b05083
33. N. Liu et al., Grain refinement and grain coarsening of undercooled Fe-Co alloy,Mater. Charact. **57** (2006) 115–120
34. H. Nitta et al., Grain boundary self-diffusion in directionally solidified equiatomic Fe-Co alloy,Mater. Sci. Eng. A **382** (2004) 250–256
35. Z. Li et al.,Effect of punching edge deformation on the magnetic properties of Fe49-Co49-V2 alloy, J. Magn. Magn. Mater. **510** (2020) 166978
36. R.H. Yu, S. Basu, Y. Zhang, A. Parvizi-Majidi, J. Q. Xiao, Pinning effect of the grain boundaries on magnetic domain wall in FeCo-based magnetic alloys, J. Appl. Phys. **85** (1999) 6655–6659
37. S. Hasani et al., Influence of annealing treatment on micro/macro-texture and texture dependent magnetic properties in cold rolled FeCo-7.15V alloy, J. Magn. Magn. Mater. **378** (2015) 253–260
38. M. Wu, G. Yang, J. Liu, D. Yin, Y. Yang, Densification mechanism of copper micro-components prepared by the micro-forming fields activated sintering technology, J. Alloys Compd. **692** (2017) 434–439
39. K. Huang, Y. Yang, Y. Qin, G. Yang, D. Yin, A new densification mechanism of copper powder sintered under an electrical field, Scr. Mater. **99** (2015) 85–88
40. U. Anselmi-Tamburini, S. Gennari, J.E. Garay, Z. Munir, Fundamental investigations on the spark plasma sintering/synthesis process: II. Modeling of current and temperature distributions, Mater. Sci. Eng. A **394** (2005) 139–148
41. W. Chen, U. Anselmi-Tamburini, J.E. Garay, J.R. Groza, Z. Munir, Fundamental investigations on the spark plasma sintering/synthesis process: I. Effect of dc pulsing on reactivity, Mater. Sci. Eng. A **394** (2005) 132–138
42. T. Massalsk, H. Okamota, P. Subramanian, L. Kacprzak, Binary Alloy Phase Diagrams, 2nd edn. (ASM International, New York, 1990)
43. S. Fishman, R. Jeffery,Effect of High Pressure on Self-Diffusion in Concentrated FeCo Alloys,Phys Rev B. **12** (1971) 4424–4427
44. O. Guillon et al., Field-assisted sintering technology/spark plasma sintering: Mechanisms, materials, and technology developments, Adv. Eng. Mater. **16** (2014) 830–849
45. S.H. Joo, K. Yubuta, H. Kato,Ordering kinetics of nanoporous FeCo during liquid metal dealloying and the development of nanofacets, Scr. Mater. **177** (2020) 38–43
46. S. Sarkar, C. Bansal, Kinetic paths for B2 order in nanocrystalline FeCo-Mo: A Mössbauer spectroscopic study,Acta Mater. **49** (2001) 1789–1792

Cite this article as: Bohao Zhou, Yi Yang, Yi Qin, Gang Yang, Mingxia Wu, Fabrication of equiatomic FeCo alloy parts with high magnetic properties by fields activated sintering, Manufacturing Rev. **9**, 7 (2022)